

Experimental Observation of Mesoscopic Fluctuations to Identify Origin of Thermodynamic Anomalies of Ambient Liquid Water

Yukio Kajihara,^{1,*} Masanori Inui,¹ Kazuhiro Matsuda,² Daisuke Ishikawa,³ and Satoshi Tsutsui³

¹*Graduate School of Advanced Science and Engineering,*

Hiroshima University, Higashi-Hiroshima, Hiroshima 739-8521, Japan

²*Department of Physics, Kumamoto University, Kumamoto 860-8555, Japan*

³*Japan Synchrotron Radiation Research Institute (JASRI) Sayo-cho, Hyogo 679-5198, Japan*

(Dated: November 15, 2021)

We report a new experimental approach for observing mesoscopic fluctuations underlying the thermodynamic anomalies of ambient liquid water. In this approach, two sound velocity measurements with different frequencies, namely inelastic X-ray scattering (IXS) in the terahertz band and ultrasonic (US) in the megahertz band, are required to investigate the relaxation phenomenon of sound waves with the characteristic frequency between the two aforementioned frequencies. We performed IXS measurements to obtain the IXS sound velocity of liquid water from the ambient conditions to the supercritical region of liquid-gas phase transition (LGT) and compared the results with the US sound velocity reported in the literature. We found that the ratio of the sound velocities, S_f , which corresponds to the relaxation intensity, obtained using these two methods exhibits a simple but significant change. Two distinct rises were observed in the high-temperature and low-temperature regions, implying that two relaxation phenomena exist. In the high-temperature region, a peak was observed near the LGT critical ridge line, which was linked with changes in the magnitude of density fluctuation and isochoric and isobaric specific heat capacities. This result indicates that the high-temperature relaxation originates from the LGT critical fluctuation, proving that this method is effective for observing such mesoscopic fluctuations. Meanwhile, in the low-temperature region, S_f increased from 550 K toward the low-temperature region and reached a high value, attaining the “fast sound” state near ambient conditions. This result indicates that another mechanism of relaxation exists, which causes the sound velocity anomaly, including the “fast sound” phenomenon of liquid water near ambient conditions. The change in S_f in the low-temperature region is linked with the change in the isochoric heat capacity, which implies that this relaxation causes the well-known heat capacity anomaly of liquid water. This low-temperature relaxation corresponds to the critical fluctuation of the liquid–liquid phase transition (LLT) that is speculated to exist in the supercooled region. In this study, both LGT and LLT critical fluctuations were observed, and the relationship between thermodynamics and the critical fluctuations was comprehensively discussed by analyzing the similarities and differences between the two phase transitions.

I. INTRODUCTION

The thermodynamic behaviors of some “anomalous liquids” differ considerably from those of other liquids. The most well-known case is of water near ambient conditions. The density of liquid water is the greatest at a temperature slightly above its melting temperature; the slope of the melting curve against pressure is negative, and the heat capacity shows a divergence-like increase in the supercooled region. The (ultrasonic (US) or adiabatic) sound velocity increases with the temperature and reaches its maximum value at approximately 350 K. Many scenarios have been proposed to explain the thermodynamic anomalies of liquid water; however, a solution has not been determined. A liquid–liquid phase transition (LLT) scenario (or a liquid–liquid critical point (LLCP) hypothesis [1, 2]) is regarded as the most promising scenario [3, 4]. In this scenario, two structures exist in liquid water with a discontinuous (first-order-like) phase transition between them, which may have its own criti-

cal point in the high-pressure and deep supercooled region. Ambient water is located in the LLT supercritical region; its thermodynamic features are strongly affected by the LLT “critical fluctuation,” which causes anomalies. For such an LLT scenario, many theoretical and simulation studies have preceded experimental investigation. For example, Anisimov’s group constructed a thermodynamic equation by assuming LLCP and quantitatively reproduced many thermodynamic quantities, such as density, heat capacity, surface tension, and sound velocity (of zero-frequency limit), measured in the liquid region, including the supercooled region [5]. However, the estimated critical pressure of LLCP, which is approximately zero, may be too low compared with the values estimated by other researchers (approximately 50 [6, 7] to 150 MPa [1, 8]). Furthermore, some of the estimated properties, such as compressibility, isochoric heat capacity, and sound velocity, exhibit unphysical features near LLCP. It is uncertain if a critical point really exists. In this sense, a two-order-parameter model proposed by Tanaka may be more appropriate. In the model, the existence of two states or two structural orderings is assumed; however, it does not necessarily assume an LLCP or real (first-order-like) LLT between these two orderings. By

* kajihara@hiroshima-u.ac.jp

introducing a frustration of the two orders, it is possible to quantitatively explain not only the many thermodynamic anomalies of liquid water [9] but also other properties of various liquids, such as glass transition, using simulation techniques [10].

To prove the LLT scenario or to solve the problem of the thermodynamic anomalies of water, clear experimental results are necessary. However, although more than a quarter of a century has passed since the scenario was proposed [1] and numerous experiments have been subsequently conducted, conclusive evidence is yet to be obtained [3]. This is mainly because the real first-order-like LLT and LLCP are expected to be located in the deep supercooled “no-man’s land” [2] at high pressure, where real experiments cannot be conducted. However, we believe that there is a method to prove the LLT concept without reaching the no-man’s land. This method involves observing the “critical fluctuation” that are believed to be widely spread around the LLCP or LLT and predicting the LLCP from this spread. Analogously, even when the top of Mt. Everest is covered with clouds, if we find a path (a ridge) and follow this path upward, we can move toward the summit [11]. In principle, it is not clear what physical quantities are good indexes for LLT critical fluctuation. In the case of the liquid–gas transition (LGT) critical fluctuation, the magnitude of density fluctuation is widely recognized as a good index, which can be measured through small-angle scattering experiments using X-rays (SAXS) and neutrons (SANS). SAXS and SANS measurements of liquid water have shown that the small-angle scattering intensity increases toward low temperatures, including the supercooled region [12]. A hydrogen-bond network [13, 14], a clustering [15], and recently, the existence of two structures [16] have been discussed. This interpretation has been controversial for many years [17]; however, Nilsson’s group made a breakthrough using the state-of-the-art X-ray free electron laser (XFEL). They succeeded in going into the deep supercooled no-man’s land and claimed to have observed the maximum of the integrated scattering intensity, indicating the existence of LLT [18]. Although caution is still exercised when recognizing this result as the maximum [19], the rise certainly stagnated. To confirm the existence of LLCP or determine the critical pressure, similar SAXS measurement in no-man’s land at high pressure is desired; however, it is nearly impossible to perform XFEL experiments under pressurized conditions. Alternatively, if critical fluctuation is interpreted as the coexistence of two phases, another experimental verification is possible. Over a century ago, Röntgen claimed that liquid water consists of two different local structures [20]; however, it is fundamentally impossible to prove this through normal diffraction measurement [21] because the obtained structure factor is spatially averaged. Nevertheless, notable experimental result on the two structures in liquid water is as follows: they are not actual particle structures but electronic structures. The oxygen K-edge X-ray emission spectra of liquid water exhibit two distinct peaks [22–

24] that are thought to correspond to the two structures assumed in the LLT scenario. The temperature variations of the intensities of these peaks are consistent with the scenario, which was subsequently extended to the supercooled no-man’s land using the XFEL technique [25]. Similar results and discussions have been reported for X-ray absorption spectra [26, 27], although the resolution is not as high as that of XES spectra. These results provide strong evidence of coexistence of two phases; however, each spectrum can be interpreted differently (see [28] and Section 4.1 in [3]), and the verification is not conclusive.

Therefore, we focus on another measurement method to detect fluctuations in liquids for replacing the density fluctuation measurement, namely small-angle scattering [29, 30]. In this method, a phenomenon called “fast sound” [31, 32] was used. The velocity of sound in liquid water under ambient conditions was determined to be approximately 1500 m/s through *macroscopic* methods such as the US technique, and approximately 3000 m/s through *microscopic* methods such as molecular dynamics simulation and inelastic neutron scattering (INS). There have been several conflicting discussions [31, 32] about the interpretation of this fast-sound phenomenon of liquid water. The IXS [33] and inelastic ultraviolet scattering (IUVS) techniques [34] have revealed that the two sound velocities are connected in the small Q region and that the cause of the large difference between them is a relaxation phenomenon with high relaxation intensity. However, the cause of the large relaxation intensity and this relaxation phenomenon have not been discussed extensively. Only a few remarks state that the relaxation is related to the “making (forming) and breaking of hydrogen bonds” [31–33]. Moreover, this phenomenon has been rarely discussed or even cited by researchers studying thermodynamic anomalies. This may be unavoidable because fast-sound involves the problem of very-high-frequency sound. This, in principle, is beyond the scope of thermodynamics, which focuses on long-time-limit phenomena. We focus on this fast-sound phenomenon for verifying the LLT concept or LLCP hypothesis [30] because it is commonly observed in liquid Te [29], which shows thermodynamic anomalies similar to water [35] and is expected to have LLT in the supercooled region [36–38]. This phenomenon has also been observed around the metal–nonmetal transition region of fluid Hg [39] and is likely to be an essential element of phase transition. We previously proposed that this fast-sound could be used as a good index of LLT critical fluctuation for liquid Te [29]. To advance this proposal, we performed IXS measurements on liquid water and discussed the relationship between fast-sound and thermodynamics. In the present study, we extend the measurement region not only to the vicinity of the melting point but also to the LGT supercritical region under high-temperature and high-pressure conditions to discuss the LLT critical fluctuation, which is an unknown fluctuation, based on the results of the LGT critical fluctuation,

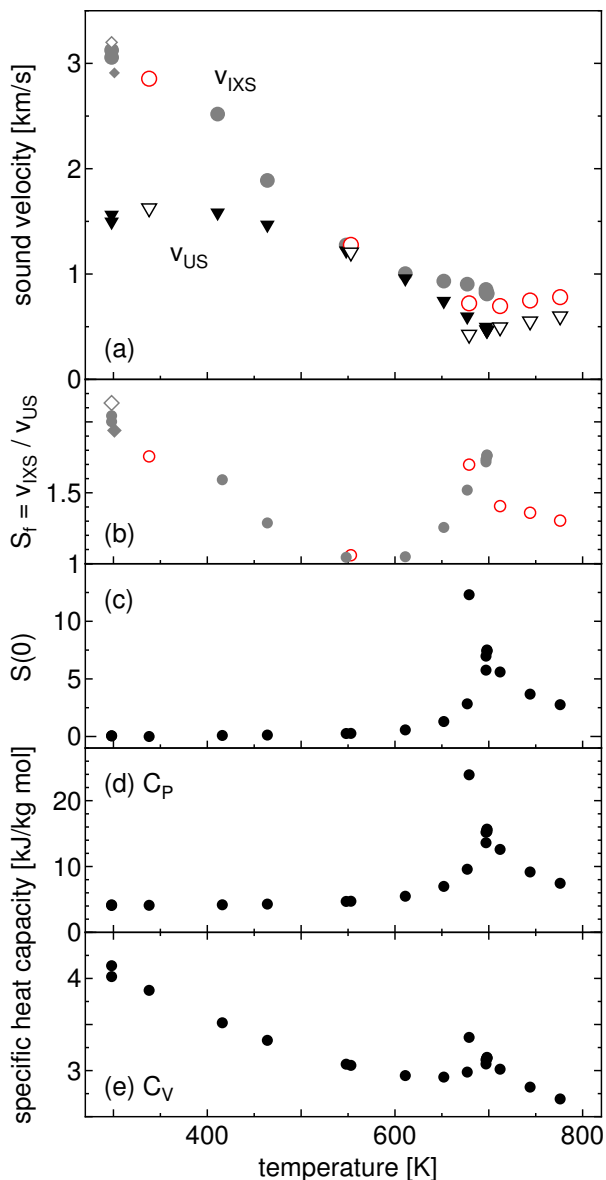


FIG. 2. (a) Temperature variation of IXS sound velocities obtained in the present study and those obtained by Yamaguchi are represented by red and gray circles, respectively. IXS sound velocities by Sette [33] and Ishikawa [42] at ambient conditions are also plotted by open and closed gray diamonds, respectively. The corresponding US sound velocity v_{US} is represented by the triangles. From these two sound velocities, (b) the strength of the fast-sound S_f parameter is calculated. Note that the horizontal axis represents the temperature; however, the pressure is not necessarily the same (Figure 1). Some thermodynamic parameters of liquid water corresponding to the state points of the measurements are also indicated: (c) zero-wavenumber structure factor $S(0)$ and specific heat capacities of (d) isobaric C_P and (e) isochoric C_V . Further, v_{US} , $S(0)$, C_P , and C_V are calculated using the IAPWS-95 formula [43].

not change uniquely with respect to the temperature.

Regarding v_{IXS} , although there are small differences between ours and others, the values are nearly consistent and have no significant effect on the following discussion; hence, we will consider them together. A very high velocity of approximately 3 km/s was observed near ambient conditions; however, nearly linear deceleration was observed as the temperature increased to approximately 550 K. This change is simple and reveals no anomalies. At high temperatures, the change becomes gradual. In addition, the red circles at 700 K and higher measured on the critical isochore line indicate that the value remains nearly constant. When the density is constant, the sound velocity is also constant, indicating a normal behavior. By contrast, the behavior of v_{US} is not normal. It rises in the region from 300 to 350 K despite the increase in temperature, and even if the temperature rises to approximately 550 K, the temperature dependence is extremely low. Furthermore, v_{US} is nearly equal to v_{IXS} around this region. At higher temperatures, the temperature dependence becomes relatively steep, and a drop can be observed near the critical isochore line (700 K at 40 MPa; Figure 1).

For seemingly contradictory changes in both sound velocities, plotting their ratio or the strength of fast sound $S_f \equiv v_{IXS}/v_{US}$ in Fig. 2(b) provides a clear indication. Specifically, S_f is a relaxation intensity in a sound wave, as will be described in Section IV A. In the high-temperature region, S_f exhibits a large peak around the critical isochore line at 700 K. Further, S_f rises significantly toward the low-temperature region. Then, in the region around 550 K, S_f is nearly 1, i.e., no fast-sound phenomenon occurred. This result shows that there are two origins of the observed fast-sound or relaxation phenomena: one is centered at approximately 700 K and the other is in the low-temperature (probably supercooled) region. Figure 1 presents a schematic representation of these origins, denoted by the monochrome and colored hatched areas in the phase diagram. It is clear that the origin in the high-temperature region is due to the LGT critical fluctuation. To confirm this, we present a comparison with other thermodynamic quantities. Figure 2 shows the (c) magnitude of (number) density fluctuation $S(0) = \rho_N k_B T \beta_T$ (where ρ_N is the number density, k_B is the Boltzmann constant, and β_T is the isothermal compressibility), (d) isobaric (constant pressure) specific heat capacity C_P , and (e) isochoric (constant volume) specific heat capacity C_V . In the high-temperature region, (c) $S(0)$ peaks at approximately 700 K owing to the LGT critical density fluctuation. The specific heat capacities (d) C_P and (e) C_V also show peaks at approximately 700 K, similar to $S(0)$. These temperature dependences are nearly linked to S_f , and it is concluded that the fast-sound phenomenon in the high-temperature region is due to the LGT critical fluctuation.

Meanwhile, in the low-temperature region, S_f shows a substantial increase from approximately 550 K toward room temperature. This indicates that there exists another origin distinct from LGT for this fast-sound phe-

nomenon in the low-temperature region. The phase diagram in Fig. 1 reveals that the phenomenon in the low-temperature region is caused by LLT or LLC which speculated to exist in the supercooled region. Conversely, the increase in S_f is a good indicator of LLT or LLC hidden in no-man's land. The area of the phenomenon of LLT seen in the S_f parameter is considerably wider than that of LGT. The difference between the fast-sound phenomenon in the low-temperature region and that of LGT is that the S_f parameter does not seem to be linked with the density fluctuation $S(0)$ (Fig. 2(c)) and isobaric specific heat capacity C_P (Fig. 2(d)). By contrast, the temperature dependence of the isochoric specific heat capacity C_V (Fig. 2(e)) suggests that it is also similar to S_f . Moreover, C_V shows a peak at approximately 700 K in the high-temperature region, which implies that it reflects the critical fluctuation of LGT; however, the low-temperature range clearly suggests that it increases with cooling even at 550 K or lower. In addition, the absolute value is also larger in the low-temperature range than in the high-temperature range, which is similar to the behavior of S_f . This feature is a new finding that has not been reported previously. We will discuss this point further in Sections IV B and IV C.

IV. DISCUSSION

In this section, we discuss the relationship between the obtained S_f parameter and thermodynamics while focusing on the fluctuations. Before discussing the actual experimental data, we first review the basic concepts. In Section IV A, we first review the characteristics of the relaxation phenomenon in sound waves and discuss the physical meaning of S_f , which is introduced in the present paper, while focusing on its time and length scales. We explain that the proposed method can detect dynamical fluctuations at the mesoscopic level. In Section IV B, we show the wide range of temperature and pressure dependences of some thermodynamic quantities to present an overview of the thermodynamics and clarify the anomalies near ambient conditions. Based on these two concepts, we comprehensively discuss the relationship between the present experimental results, thermodynamics, and relaxation phenomena, while focusing on the fluctuations in Section IV C. We attempt to discuss the thermodynamics of liquid water from a novel perspective.

A. Relaxation of sound wave and mesoscopic fluctuation

In this section, we review the relaxation phenomenon of sound waves to understand the physical meaning of the phenomenological parameter S_f introduced in this study. Figure 3 schematically shows the relaxation curve of sound waves. The vertical axis represents the sound ve-

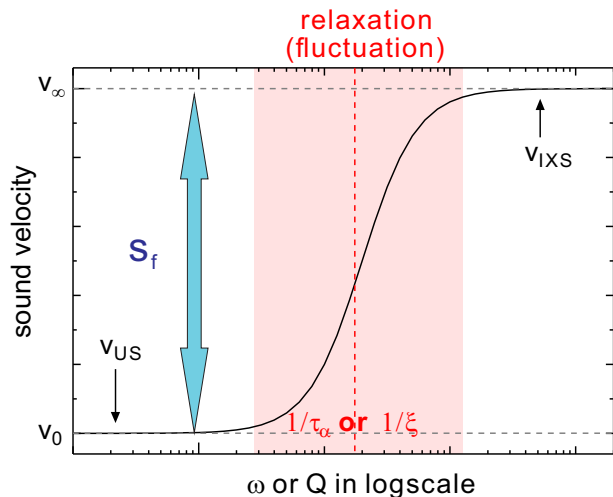


FIG. 3. Schematic illustration of the relaxation curve of sound waves. When there exists a certain relaxation or fluctuation with a characteristic time (τ_α) or spatial size (ξ), the measured sound velocity has a high value in the high-frequency region and a low value in the low-frequency region. In general, the frequency of IXS is significantly higher and that of US is significantly lower than the characteristic frequency of the relaxation. We define the ratio of these two sound velocities as S_f .

locity, while the horizontal axis represents the frequency ω for the relaxation phenomenon in general. However, in the case of sound waves, the frequency and wavenumber (momentum transfer Q in terms of measurement) are nearly proportional; hence, Q can be used. When there is a certain relaxation phenomenon in the system, the velocity will be measured as a higher value v_∞ at higher ω (or higher Q) and lower value v_0 at lower ω (or lower Q), with the inverse of its characteristic time τ_α (length ξ) as a boundary. Alternatively, it is possible to interpret that the sound velocity at low frequency is reduced from that at high frequency owing to the existence of the relaxation phenomenon. We define the relaxation intensity as

$$\epsilon \equiv \frac{v_\infty - v_0}{v_0}. \quad (1)$$

Meanwhile, Fig. 4 shows the energy transfer ($E = \hbar\omega$, where \hbar is the reduced Planck constant) and Q region covered by some dynamics measurement methods. IXS is located in the highest E and Q region, and it is generally used to observe the local motion of atoms and molecules, whose characteristic frequency is of the order of terahertz. By contrast, the frequency of the US wave is in the megahertz region and is located in the lowest E and Q region in this figure. The solid blue line in the figure represents the representative dispersion relation of the sound velocity. It ranges from approximately 500 to 5000 m/s for most liquids, and if the region between these dotted lines can be measured, the relaxation curve shown in Fig. 3 will be completed. In general, the mesoscopic fluctuation or relaxation region, which is important in

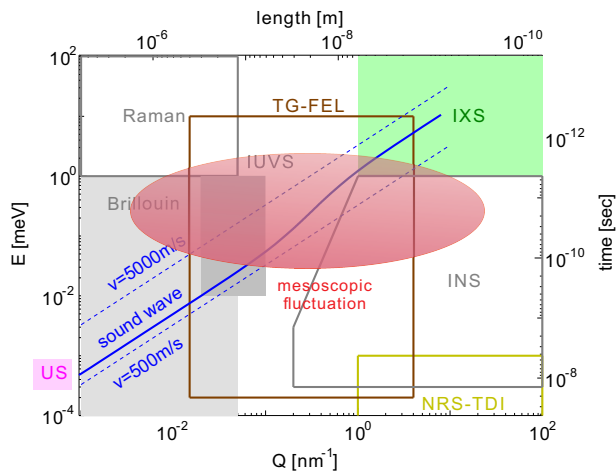


FIG. 4. Energy and momentum transfer (time and length) region of various experimental methods. The propagation of a sound wave in a liquid medium is indicated by the solid blue line in the area between the two dashed lines. Mesoscopic fluctuations, which are critical in liquids, exist around the red ellipse. IXS and US are the largest and the lowest Q and E regions, respectively, in this range, and a large gap exists between them. Light scattering methods (Raman, Brillouin, and IUVS) can fill this gap to a certain extent and TG-FEL [44, 45] is expected to fill a considerable part. INS and nuclear resonant scattering using time-domain interferometry (NRS-TDI[46–48]) are also important for measuring the dynamics of liquids.

disordered systems such as liquids, is located in the region shown by the red ellipse. The existence of such a mesoscopic relaxation phenomenon reduces the sound velocity only in the lower ω (or Q) region. In general, US has a sufficiently low ω (or Q) and IXS has a sufficiently high ω (or Q) compared to the mesoscopic fluctuation, whose characteristic frequency is $1/\tau_\alpha$ (Q is $1/\xi$). Then, the relaxation intensity is approximated as

$$\epsilon \simeq \frac{v_{\text{IXS}} - v_{\text{US}}}{v_{\text{US}}} = S_f - 1. \quad (2)$$

Therefore, the strength of fast-sound S_f corresponds to the relaxation intensity ϵ . We propose such a relaxation-intensity-measurement method (or fast-sound-measurement method based on the historical background) using two sound velocity measurements of different frequencies, namely US and IXS, together, as a new experimental method to characterize liquids. The advantage of this method is that only the ratio of v_{US} and v_{IXS} is required and no complex analysis is involved. Another advantage is that it can grasp the total intensity of relaxations, whose characteristic frequencies range from the megahertz band to the terahertz band, even if the entire relaxation curve cannot always be measured. In the present IXS measurement of water, the deduced Q -dependent velocity $v(Q)$ gradually approaches v_{US} in the low Q region, which means that a part of the “mesoscopic” relaxation is located in the IXS measurement

range. However, this mesoscopic region is nearly completely out of the IXS range for liquid water at the lower temperature [34] or liquid Te, which is a similar system exhibiting LLT [29]. In such a case, it is usually desirable to measure the relaxation region by combining other measurement methods. However, in practice, there is a gap in the E and Q region that is not covered by any measurement method. The free electron laser-based transient grating spectroscopy (TG-FEL) [44, 45], which nearly covers this gap region, as shown in Fig. 4, could be a highly effective and ambitious approach; however, it has not been completely developed thus far. In any case, it is usually not realistic to measure the entire relaxation curve. Even in these situations, the S_f parameter obtained by the relaxation-intensity-measurement method is effective. Moreover, the shape of the relaxation curve and the number of relaxation phenomena in the frequency range between the megahertz and terahertz bands are irrelevant. This is because the relaxation curve in the sound wave is connected by a single curve from the microscopic region to the macroscopic region. We believe that this method is highly effective for detecting relaxation phenomena or fluctuations in mesoscopic scales.

B. Pressure and temperature dependences of thermodynamic quantities

In this section, we present an overview of thermodynamic quantities by considering a wide range of temperature and pressure dependences. In liquid water, the thermodynamic quantities in temperature and pressure ranges up to 1273 K and 1000 MPa, respectively, are expressed and can be obtained by an empirical formula, namely the IAPWS-95 formula, which was constructed based on a large amount of experimental data [43]. The values from this equation are shown in the Fig. 2 presenting the experimental results. The temperature and pressure dependences (contour map) of some parameters that are important for the present discussion are stated below. Note that, in the original paper, only mathematical formula or tabulated values were listed and no figures were provided for visually grasping the overview of thermodynamics. First, Fig. 5 plots the isochoric heat capacity C_V , which is a vital parameter [49] in thermodynamics. The LGT critical point is located at 647 K and 22 MPa. In Area 1, C_V forms a thin linear peak centered on this critical point. It is reasonable to recognize this spread as the LGT critical fluctuation. Meanwhile, in the low-temperature region in Area 2, there is a large mountain peak centered near ambient conditions (probably supercooled region), whose behavior is totally different from that of the peak in the high-temperature region. Remarkably, this peak extends over a fairly high-temperature and high-pressure region up to 1000 MPa, which has a dominant effect on C_V in nearly the left-half region of this figure. Another notable feature is that the LGT critical fluctuation showed a sharp and nar-

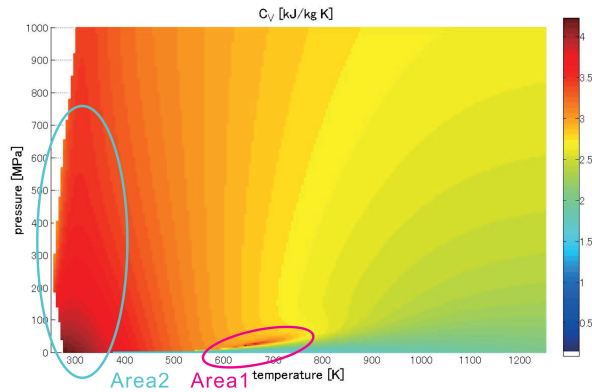


FIG. 5. Contour map of isochoric heat capacity C_V . Areas 1 and 2, indicated by the red and sky-blue ellipses, represent the LGT critical region and low-temperature- C_V -mountain region, respectively.

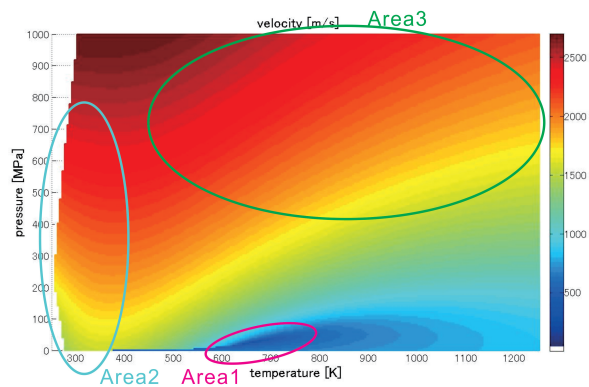


FIG. 6. Contour map of (adiabatic or US) sound velocity. Areas 1, 2, and 3, indicated by the red, sky-blue, and green ellipses, represent the LGT critical area, low-temperature- C_V -mountain area, and “normal” area, respectively.

row spread in the direction of the ridge line; however, the “low-temperature C_V mountain” does not have such a direction. Apparently, the well-known anomaly of the specific heat capacity of liquid water near ambient conditions is due to this low-temperature- C_V -mountain. Further details on this low-temperature- C_V -mountain will be provided at the end of this section and in the next paper [49]. Next, we will consider the sound velocity. Although there is no particular description about the feature of the “speed of sound” in the original paper [43], most of the original experimental data are obtained using the US method; hence, it is reasonable to recognize this as US sound velocity v_{US} , demonstrated in Fig. 6. Considering Area 3 at sufficiently high temperature and pressure, it can be seen that v_{US} decreases nearly linearly as the temperature increases and the pressure decreases, which is a “normal” variation. Considering the LGT critical area (Area 1), it can be clearly seen that v_{US} decreases significantly around the LGT critical point compared to

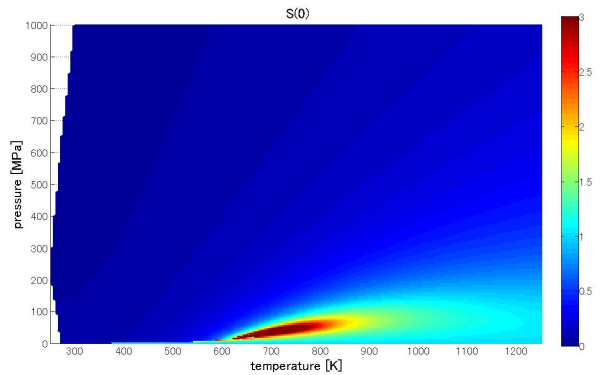


FIG. 7. Contour map of density fluctuation parameter $S(0)$.

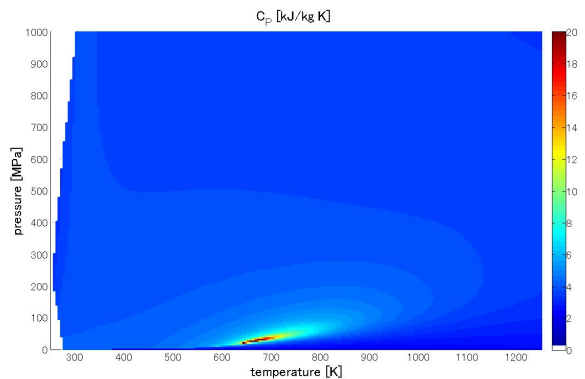


FIG. 8. Contour map of isobaric heat capacity C_P .

the surrounding area. This decrease is linked with the increase in C_V seen in Fig. 5. Therefore, (the decrease in) v_{US} is also a good indicator of the LGT critical fluctuation. Meanwhile, the low-temperature Area 2 should be noted. It can be seen that v_{US} clearly decreases compared to the “normal” changes in Area 3. The spread of this decrease area is nearly linked with the spread of the low-temperature- C_V -mountain in Fig. 5. Thus, the decrease in v_{US} (Fig. 6) and the anomaly of sound velocity near ambient conditions, showing the maximum value at approximately 350 K as stated in the Introduction section, have the same origin as this low-temperature- C_V -mountain.

As displayed previously, this low-temperature- C_V -mountain depicts the thermodynamic anomalies of liquid water near ambient conditions. The fact that C_V forms a mountainous peak and is related to the decrease in US sound velocity is identical to the LGT critical fluctuation. Therefore, this anomaly can be regarded as LLT critical fluctuation; however, the difference from the LGT critical fluctuation should be studied. The behaviors of the magnitude of the density fluctuation $S(0)$ (Fig. 7) and isobaric heat capacity (Fig. 8), which are known as good indicators of LGT critical fluctuation, are significantly different in the low-temperature region. Both param-

ters exhibit sharp thin linear peaks near the LGT critical point, whereas a slight effect is observed in the low-temperature region on this scale. To solve this paradox, it is necessary to expand the region near ambient conditions. Figure 9 shows the temperature dependences of (a) $S(0)$ and (b) heat capacities (C_P and C_V) at pressures of approximately 0.1 (black lines) and 40 MPa (red lines). The lines are plotted using the IAPWS-95 formula [43],

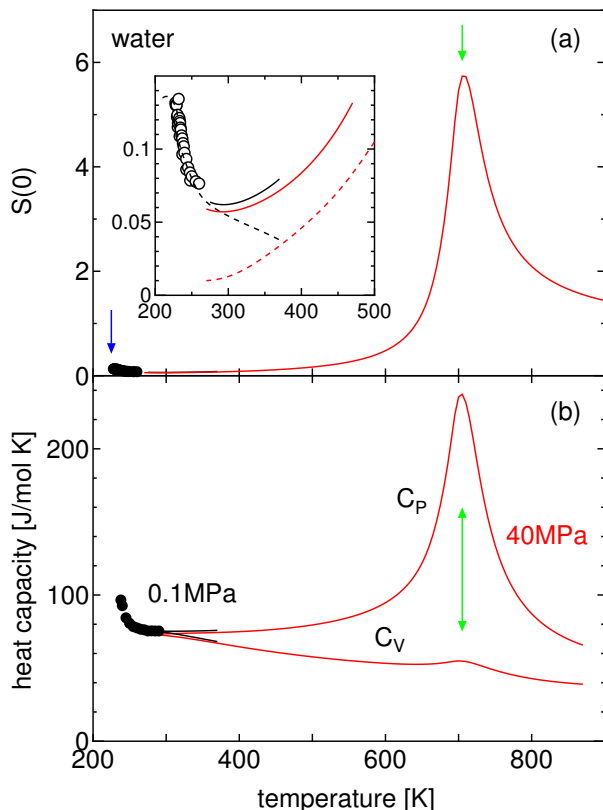


FIG. 9. (a) $S(0)$ parameter and (b) specific heat capacities of liquid and supercooled liquid water. The red and black lines denote $S(0)$, C_P , and C_V at 40 MPa and 0.1 MPa, respectively, calculated using the IAPWS-95 formula [43]. The black circles denote experimentally obtained values of $S(0)$ [18] under the vacuum condition and C_P [50] at 0.1 MPa. The dashed lines are visual guides.

and the black symbols denote experimental values in the supercooled region [18, 50]. In particular, $S(0)$ is based on the experiment using XFEL [18], as discussed in the Introduction, and is claimed to have reached the critical ridge line of LLT, indicated by the blue arrow. In the figure, the difference in the pressure is not the essence of the discussion; hence, we will only consider the temperature dependences. In the high-temperature region, $S(0)$, C_P , and C_V all show their maximum around the LGT critical ridge line, indicated by green arrows at approximately 700 K. However, we can observe that the peak of C_V is very small compared to that of the other two parameters. Meanwhile, we focus on the low-temperature region. The data in the supercooled region are naturally connected

to the real liquid region above the melting temperature, and it is judged that there is no particular contradiction between these two data. Moreover, the supercooled liquid is not considerably different from the real liquid. It is claimed that $S(0)$ exhibits its maximum value at the LLT critical ridge in the supercooled region (blue arrow); however, it can be seen that the absolute value is negligibly small (approximately one-hundredth) compared with that at the LGT critical ridge line. This fact is an important point [51] that has not received much attention in previous LLT studies. The value can be understood with the following rough estimate. It can be assumed that in LGT, a liquid with a density of $\rho_{\text{liq}} = 1.0 \text{ g cm}^{-3}$ and a gas with a density of $\rho_{\text{gas}} = 0.0 \text{ g cm}^{-3}$, and in LLT, a liquid with a low density of $\rho_L = 1.0 \text{ g cm}^{-3}$ and a liquid with a high density of $\rho_H = 1.1 \text{ g cm}^{-3}$, become inhomogeneous; thus, the order estimation of the ratio of these two $S(0)$ values for LGT and LLT can be expressed as follows:

$$\frac{S(0)_{\text{LLT}}}{S(0)_{\text{LGT}}} \sim \frac{(\rho_H - \rho_L)^2}{(\rho_{\text{liq}} - \rho_{\text{gas}})^2} \sim 10^{-2}. \quad (3)$$

The ratio of $S(0)$ at LGT critical ridge and that at the supercooled LLT critical ridge is reasonable as the critical density fluctuation. Thus, such a comparison between LLT and LGT implies that there is an overwhelming quantitative difference in the density fluctuation even in the same critical fluctuations. This quantitative difference has a strong influence on the behavior of $S(0)$ near room temperature. With a decrease in the temperature, $S(0)$ increases sharply in the supercooled region due to LLT, which, however, is a misleading interpretation. The vicinity of room temperature is far from the LGT critical point; however, there is an influence of the tail of the LGT critical density fluctuation that is 100 times than that of the LLT critical density fluctuation. The influences of both these origins are considered, as shown in the inset of Fig. 9 (a) by the dashed lines. The influence of LLT extends to a considerably high temperature region. Near room temperature, $S(0)$ is small and no significant temperature change is observed. However, this does not necessarily mean that there is no fluctuation or temperature variation. Both LLT and LGT critical fluctuations are substantially present, and the state in which the three phases of the low-density liquid, high-density liquid, and gas are mixed every moment with respect to the temperature changes. We believe that the same can be said for C_P . The increase in C_P owing to the LLT critical fluctuation is considerably smaller than that of LGT. C_P increases sharply in the supercooled region; the stagnation near room temperature is due to the coexistence of both critical fluctuations of LGT and LLT, and it would be reasonable to assume that the influence of LLT extends to much higher temperatures. In fact, the rise in C_V begins at a much higher temperature with decreasing temperature. Further, C_V , the constant volume heat capacity, reduces the volume effect on the heat capacity, and it is considered that the effect of LLT can

be seen more easily by eliminating the effect of the overwhelmingly large density (volume) fluctuation of LGT. Based on these points, it can be concluded that the low-temperature- C_V -mountain observed in the contour map of C_V (Fig. 5) is the LLT critical fluctuation. In any case, from these contour maps, it is clear that the magnitude of the density fluctuation and C_P , which are good indicators of the LGT critical fluctuation, are no longer good indicators of the LLT critical fluctuation. Accordingly, we propose C_V and the (decrease in) US sound velocity as good indicators of both LGT and LLT critical fluctuations.

The details of these thermodynamic quantities will be further discussed in the next paper [49] from another perspective. The quantitative difference between the density fluctuation and the magnitude of the decrease in the sound velocity owing to LLT was discussed in the previous paper on liquid Te [29]. We speculate that the difference in electronic states between the two phases will be the key factor. This is natural for liquid Te, whose LLT accompanies metal–nonmetal transition. We believe that this is also common for liquid water because two peaks are observed in the X-ray emission and absorption spectra [23–27], as introduced in Section I, and an energy difference exists between the electronic states of the two phases. We believe that this is the essential difference between LGT and LLT.

C. Relationship between relaxation, thermodynamics, and critical fluctuations

Based on the background presented in the two preceding subsections, we discuss the present experimental results. As discussed in Section IV A, the fact that the S_f parameter shows a large value indicates that there exists a relaxation phenomenon having mesoscopic time and length scales. The result in Fig. 2(b) proves that there exist two relaxation phenomena in the high-temperature region and low-temperature region, and that in the high-temperature region LGT critical fluctuation clearly exists. The relaxation in the low-temperature region also exhibits a critical-like-fluctuation feature, which is notable in terms of whether it could serve as evidence of the existence of real LLT or LLC in the deep supercooled region. However, we emphasize that what both relaxation phenomena have in common is that their intensities S_f (Fig. 2(b)) are linked with C_V (Fig. 2(e)). We propose that the linkage between thermodynamics and relaxation phenomena should be regarded as a dynamical critical fluctuation and that the fluctuation itself should be focused on and discussed.

In addition to the relaxation intensity, the IXS velocity v_{IXS} itself can be discussed. As discussed in Section IV B, (US) sound velocity decreases compared with the “normal” temperature–pressure dependence in the surrounding area, owing to the effects of the LGT and LLT critical fluctuations. Meanwhile, the temperature dependence of

v_{IXS} obtained at this time is normal and unrelated to the effects of these two critical fluctuations. Given these facts, it is reasonable to consider that a sufficiently-high-frequency method such as IXS measures the “normal” sound velocity unrelated to critical fluctuations, i.e., it can invalidate or freeze the critical fluctuations. In any case, the results indicate that the mechanisms of these two critical fluctuations are relaxation phenomena, whose frequency and wavenumber scales exist in the mesoscopic region, i.e., frequency from the terahertz band to the megahertz band and wavenumber from nm^{-1} to μm^{-1} . We consider that these scales are reasonable as “critical phenomena” that accompany the phase transition. In the supercritical state, which shows substantial critical fluctuation, the two phases are considered to be in a mixed state; however, at the local or microscopic level, it should be one of the local structures. In other words, there is no particular peculiarity in a length scale of \AA and a time scale of sub-picoseconds, which reflects the strong correlation with the neighboring particles. The problem is how these local structures behave collectively, which creates the peculiarities of critical fluctuations. Naturally, the characteristics of critical fluctuations require a size that particles are grouped to some extent, which is a length scale of nanometers or more, with a time scale of picoseconds or more. In observing such collective characteristics, the sound wave should be highly effective and sensitive, because its mechanism is a collective excitation of particles.

Here, we formulate the aforementioned experimental facts. The (adiabatic) sound velocity v_S is related to the adiabatic compressibility as follows: $\beta_S = 1/(\rho v_S^2)$. Assuming that a “critical fluctuation” component β_S^f is added to the “normal” component $\tilde{\beta}_S$, it becomes

$$\beta_S = \tilde{\beta}_S + \beta_S^f. \quad (4)$$

The present experimental results are expressed as follows:

$$\beta_S = \beta_S(\omega = 0) = \frac{1}{\rho v_S^2} \simeq \frac{1}{\rho v_{\text{US}}^2} \quad (5)$$

$$\tilde{\beta}_S = \beta_S(\omega = \infty) = \frac{1}{\rho v_\infty^2} \simeq \frac{1}{\rho v_{\text{IXS}}^2} \quad (6)$$

$$\frac{\beta_S^f}{\beta_S} = \frac{\beta_S - \tilde{\beta}_S}{\beta_S} = 1 - \left(\frac{v_S}{v_\infty}\right)^2 \simeq 1 - S_f^{-2}, \quad (7)$$

and the relationship between the critical fluctuation component of adiabatic compressibility and the experimental parameter S_f is obtained. Thus, the relaxation intensity S_f is a good index for critical fluctuations. We conclude that the proposed relaxation-intensity-measurement method is effective as a method for measuring critical fluctuations regardless of LGT or LLT.

V. CONCLUDING REMARKS

We observed relaxation phenomena with mesoscopic time and length scales of liquid water from ambient conditions to the supercritical region using the newly proposed relaxation-intensity-measurement method. As a result, we observed two relaxation phenomena of different origins in the high-temperature and low-temperature regions. The relaxation intensity in the high-temperature region showed a peak near the LGT critical ridge line; the change is linked with those of the magnitude of density fluctuation and isobaric and isochoric specific heat capacities. We concluded that the relaxation corresponds to the LGT critical fluctuation. Meanwhile, the relaxation intensity in the low-temperature region increases from approximately 550 K toward the low-temperature region, which indicates that its origin exists in the supercooled region. The change is linked with the isochoric specific heat capacity, which indicates that the relaxation is the origin of the well-known heat capacity anomaly near ambient conditions. To the best of our knowledge, this is the first study in which the origin of the specific heat anomaly of liquid water was experimentally verified. It seemed natural to recognize this relaxation in the low-temperature region as the critical fluctuation corresponding to LLT or LLCP, which was proposed to exist in the supercooled region, and we discussed its validity with some evidence. We also discussed the similarities and differences between LGT and LLT critical fluctuations: the magnitude of the density fluctuation and isobaric heat capacity, which are good parameters of the LGT critical fluctuation, are not necessarily suitable for LLT; instead, we intend to propose isochoric heat capacity and the decrease in the sound velocity or relaxation intensity as effective indicators.

We believe that we have adopted a new approach for thermodynamic anomalies in liquid water, which has not been considered in previous studies. This study was motivated by the awareness of issues related to the future development of LLT research. First, we focused on the mesoscopic fluctuations. The critical fluctuation, e.g., density fluctuation for LGT, produces the divergent increase of the specific heat capacity near the critical point. To understand the thermodynamics of liquids associated with the phase transitions, the fluctuation itself is important and needs to be measured directly through experiments. In addition, except for P [52] and Se [53], in most liquid systems, such as water, Te, and Si, where LLT is assumed, the actual first-order-like LLT exists in the supercooled region, which means that only the “supercritical” state is accessible. In such a supercritical state, it is not the averaged physical quantity but the fluctuation that is important, and it is reasonable to focus on it. Second, we focused on understanding the LLT from the perspective of phase transition. In previous LLT studies, we believe that the differences and similarities compared to LGT or the ferromagnetic phase transition, which are typical examples of the phase tran-

sition, have not been resolved [30]. In fact, as a problem before the results of the present experiment, considering a wide range of thermodynamic contour maps reveals some differences between the critical fluctuations of LGT and LLT. The expansion of the temperature and pressure range of the LLT critical fluctuation extends to a much wider area than that of LGT. Furthermore, in LGT, there is a large fluctuation along the ridge line; however, in LLT, the fluctuation does not show such a direction. Based on this fact, we reconsider whether the conventional approach of examining a critical index to express a divergent tendency of the physical quantity along the ridge line is appropriate. It has also been mentioned above that we must reconsider what are the important indicators for LLT critical fluctuation. The decrease in sound velocity is a behavior that is commonly seen in both LGT and LLT critical fluctuations, and we believe that focusing on this point can be a breakthrough. To the best of our knowledge, these points have never been discussed previously. Third, we focused on the importance of the time and space concept. As discussed in Section I, the fast-sound problem has rarely been mentioned in studies on the thermodynamic anomalies of liquid water. It may be unavoidable that the conventional thermodynamics is intrinsically a theory that deals with long-time-limit phenomena and fast-sound is beyond its scope. In the present discussion, we addressed this problem by introducing the time and space concept by focusing on the relaxation phenomenon of sound velocity and linking it with the critical fluctuations. We believe that this will lead to the introduction of the time and space concept into thermodynamics in the near future. We are convinced that such a concept is very effective for understanding a “continuously broken ergodicity” [54] system, such as glass transition phenomena.

In addition, the relaxation-intensity-measurement method, which was applied to the system that shows critical fluctuations, is expected to have a wide range of applications as a general experimental method for characterizing the state of liquids. Even in liquid or melt samples that are considered to have inhomogeneity at the mesoscopic level, the density inhomogeneity is so small that small-angle scattering often fails to detect sufficient signals. In the case of such samples, large signals are expected to be obtained because this method can detect the dynamical inhomogeneity. We have already started to elucidate the thermodynamic anomalies of water–alcohol mixtures [55, 56]. We believe that this approach can be used for characterizing the melt of high entropy alloys [57, 58] and glass transition liquids [59] with dynamical heterogeneity [60].

ACKNOWLEDGMENT

The authors are grateful to A. Q. R. Baron for his dedicated experimental support. This work was supported by JSPS KAKENHI Grant Numbers 20244061

and 20K03789. The IXS measurements of liquid water were performed at the Synchrotron radiation facility of Japan (BL35XU of Spring-8) with the approval of the Japan Synchrotron Radiation Research Institute (JASRI) (Proposals No. 2008B1108).

APPENDIX

The details and analysis of the experimental data are presented in this section. Figure 10 shows the representative IXS spectra, representing (a) Q dependence at 40 MPa and 338 K and (b) T dependence at $Q=4.31 \text{ nm}^{-1}$. The green arrows represent the energy of the longitudinal acoustic mode defined by DHO analysis. In (a) the Q dependence, the energy increases rapidly as Q increases, which indicates that the sound velocity is very high. Meanwhile in (b) the temperature dependence, the spectrum rapidly widens and the position of the green arrow shifts to lower energies as heating. The state has reached the supercritical region and the density rapidly decreases. The large decrease in the excitation energy here indicates that the sound velocity decreases drastically in response to this large decrease in density. The IXS spectra $I(Q, E)$ were analyzed using the DHO model as follows:

$$I(Q, E) = \int S(Q, E) R(E - E') dE'$$

$$\left(\frac{S(Q, E)}{S(Q)} \right) = \left(\frac{E/k_B T}{1 - e^{-E/k_B T}} \right) \times$$

$$\left[\frac{A_L}{\pi \Gamma_L} \frac{\Gamma_L}{E^2 + \Gamma_L^2} + \sum_i^n \frac{A_{\text{DHO},i}}{\pi \hbar/k_B T} \frac{4\Gamma_{\text{DHO},i} \sqrt{E_{\text{DHO},i}^2 - \Gamma_{\text{DHO},i}^2}}{(E^2 - E_{\text{DHO},i}^2)^2 + 4\Gamma_{\text{DHO},i}^2 E^2} \right]. \quad (8)$$

Here, $S(Q, E)$ and $R(E)$ represent a model function of the dynamic structure factor of the sample and a resolution function experimentally determined with a standard material (PMMA), respectively. Further, A_L and Γ_L are the amplitude and width of the central Lorentzian, respectively; $A_{\text{DHO},i}$, $\Gamma_{\text{DHO},i}$, and $E_{\text{DHO},i}$ are the amplitude, width, and energy of the i -th DHO excitation for a total of n , respectively. We optimized the parameters using a nonlinear least-squares method by setting $n = 1$ in this equation (1-DHO model); however, near ambient conditions, since the existence of another (transverse acoustic) mode was proposed [32, 33], we also used a model with $n = 2$ (2-DHO model) to investigate the effect on the longitudinal sound velocity. Figure 11 (a) shows the result of fitting $S(Q, E)$ at 40 MPa and 338 K. The experimental data (gray circles with error bars) were well fitted by the model function (bold red line) with the Lorentzian term (blue dotted line) corresponding to quasi-elastic scattering and the DHO term (green dotted line) corresponding to inelastic scattering. From the energy position of the DHO term, the Q -dependent longitudinal sound velocity can be determined by $v(Q) = E_{\text{DHO},i=1}(Q)/E$. As shown in Fig. 11 (b), even when we adopted the 2-DHO model, which considered the longitudinal (DHO1 in the figure) and the second (DHO2) modes by setting $n = 2$ in Equation 8,

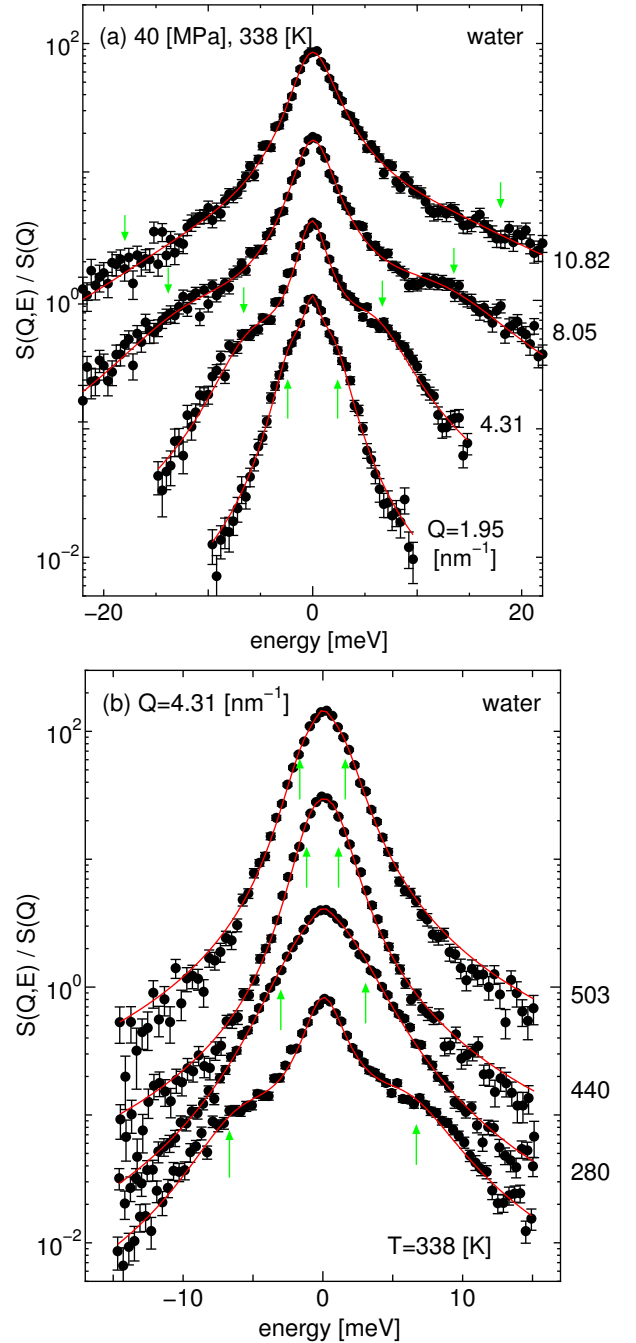


FIG. 10. Normalized dynamic structure factor of liquid water. (a) Q variation at 40 MPa and 338 K, and (b) T variation at $Q=4.31 \text{ nm}^{-1}$. The Q and T values are indicated in the figure. Each spectrum is slightly shifted for clarity. The green arrows represent the excitation energies determined by 1-DHO analysis.

the energy position of DHO1 was not significantly different. We do not believe that the model difference or the existence of the second mode is a critical problem in the present discussion. Figure 12 (a) shows the dispersion relation of the longitudinal mode at 40 MPa and 338 K.

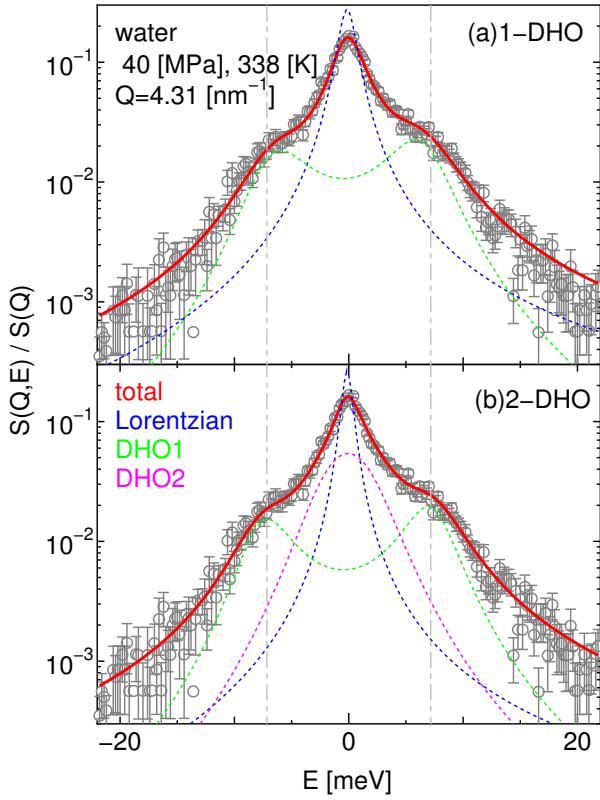


FIG. 11. Fitting results of the dynamic structure factor of liquid water at 40 MPa, 338 K, and $Q = 4.31 \text{ nm}^{-1}$, by (a) 1-DHO and (b) 2-DHO model. The gray circles and solid red line represent the experimental and fitting results, respectively. The dashed blue, green, and pink lines represent the Lorentzian, DHO1, and DHO2 components, respectively. The vertical gray dot-dashed line represents the energy of DHO1 in 2-DHO model.

With respect to Q , the energy increases nearly linearly, which confirmed that it is a longitudinal acoustic mode. The results of both the 1-DHO (black circles) and 2-DHO (blue circles) models are shown; however, no significant difference was seen. In addition, (b) is the Q -dependent sound velocity $v(Q)$ corresponding to the energy. In the high Q region above 8 nm^{-1} , the value was nearly constant, and v_{IXS} was determined by the average value in this region. The values v_{IXS} of the 1-DHO and 2-DHO models were 2.86 and 2.90 km/s, respectively, and the difference depending on the analysis model was not a major problem within the range of the error bar. There was a large difference between the absolute values of v_{IXS} and v_{US} , which is in the fast-sound state; however, they are continuously connected in the low Q region. This result indicated that the difference between the two velocities is due to the relaxation phenomenon, whose characteristic spatial size ($\simeq 2\pi/Q$) is of the order of nanometers. We performed a similar analysis on all the temperature and pressure data and determined v_{IXS} , as shown in Fig. 2 (a) by circles.

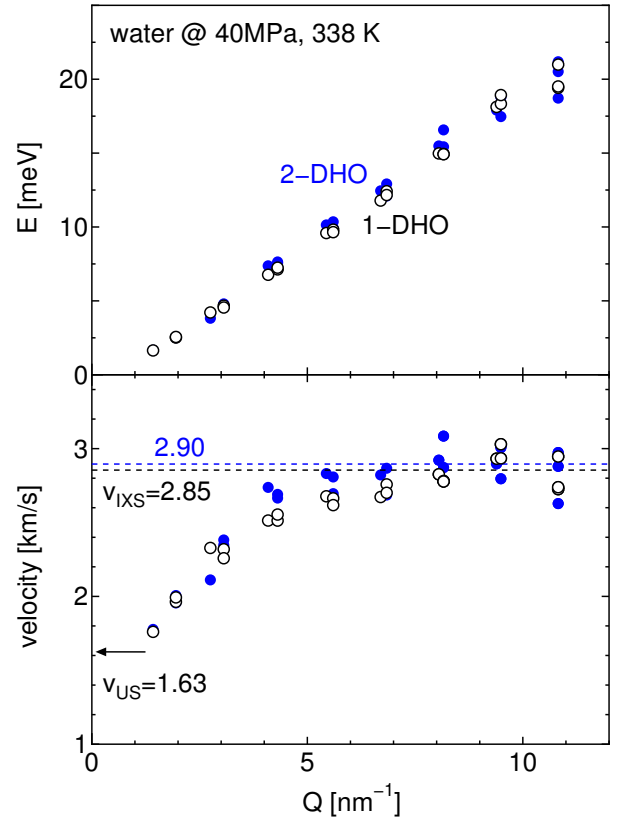


FIG. 12. (a) Dispersion curve of excitation energy and (b) Q -dependent sound velocity for liquid water. The black open and blue closed circles correspond to 1-DHO and 2-DHO models, respectively. v_{IXS} is determined in the selected Q -range ($7.5 < Q < 11 \text{ nm}^{-1}$). v_{US} is the sound velocity calculated using the IAPWS-95 formula [43].

- [1] P. H. Poole, F. Sciortino, U. Essman, and H. E. Stanley, *Nature* **360**, 324 (1992).
- [2] O. Mishima and H. E. Stanley, *Nature* **396**, 329 (1998).
- [3] P. Gallo, K. Amann-Winkel, C. A. Angell, M. A. Anisimov, F. Caupin, C. Chakravarty, E. Lascaris, T. Loerting, A. Z. Panagiotopoulos, J. Russo, J. A. Sellberg, H. E. Stanley, H. Tanaka, C. Vega, L. Xu, , and L. G. M. Pettersson, *Chem. Rev.* **116**, 7463 (2016).
- [4] H. Tanaka, *J. Chem. Phys.* **153**, 0130901 (2020).
- [5] V. Holten, J. V. Sengers, and M. A. Anisimov, *J. Phys. Chem. Ref. Data* **43**, 043101 (2014).
- [6] O. Mishima, *J. Chem. Phys.* **133**, 144503 (2010).
- [7] D. A. Fuentevilla and M. A. Anisimov, *Phys. Rev. Lett.* **97**, 195702 (2006).
- [8] L. Liu, S. H. Chen, A. Faraone, C. W. Yen, and C. Y. Mou, *Phys. Rev. Lett.* **95**, 117802 (2005).
- [9] H. Tanaka, *J. Chem. Phys.* **112**, 799 (2000).
- [10] H. Tanaka, *Euro. Phys. J. E* **35**, 113 (2012).
- [11] P. Gallo and H. E. Stanley, *Science* **358**, 6370 (2017).
- [12] R. W. Hendricks, P. G. Mardont, and L. B. Shaffert, *J. Chem. Phys.* **61**, 319 (1974).
- [13] L. Bosio, J. Teixeira, and H. E. Stanley, *Phys. Rev. Lett.* **46**, 597 (1981).
- [14] L. Bosio, J. Teixeira, and M. C. Bellissent-Funel, *Phys. Rev. A* **39**, 6612 (1989).
- [15] Y. Xie, K. F. Ludwig, Jr., G. Morales, D. E. Hare, and C. M. Sorenson, *Phys. Rev. Lett.* **71**, 2050 (1993).
- [16] C. Huang, K. T. Wikfeldt, T. Tokushima, D. Nordlund, Y. Harada, U. Bergmann, M. Niebuhr, T. M. Weiss, Y. Horikawa, M. Leetmaa, M. P. Ljungberg, O. Takahashi, A. Lenz, L. Ojamäe, A. P. Lyubartsev, S. Shin, L. G. M. Pettersson, and A. Nilsson, *Proc. Natl. Acad. Sci.* **106**, 15214 (2009).
- [17] G. N. I. Clark, G. L. Hura, J. Teixeira, A. K. Soper, and T. Head-Gordon, *Proc. Natl. Acad. Sci.* **107**, 14003 (2010).
- [18] K. H. Kim, A. Späh, H. Pathak, F. Perakis, D. Mariedahl, K. Amann-Winkel, J. A. Sellberg, J. H. Lee, S. Kim, J. Park, K. H. Nam, T. Katayama, and A. Nilsson, *Science* **358**, 1589 (2017).
- [19] F. Caupin, V. Holten, C. Qiu, E. Guillermin, M. Wilke, M. Frenz, J. Teixeira, and A. K. Soper, *Science* **360**, eaat1634 (2018).
- [20] W. C. Röntgen, *Ann. Phys.* **45**, 91 (1892).
- [21] M. Leetmaa, K. T. Wikfeldt, M. P. Ljungberg, M. Odellius, J. Swenson, A. Nilsson, and L. G. M. Pettersson, *J. Chem. Phys.* **129**, 084502 (2008).
- [22] O. Fuchs, M. Zharnikov, L. Weinhardt, M. Blum, M. Weigand, Y. Zubavichus, M. Bär, F. Maier, J. D. Denlinger, C. Heske, M. Grunze, and E. Umbach, *Physical Review Letters* **100**, 027801 (2008).
- [23] T. Tokushima, Y. Harada, O. Takahashi, Y. Senba, H. Ohashi, L. G. M. Pettersson, A. Nilsson, and S. Shin, *Chem. Phys. Lett.* **460**, 387 (2008).
- [24] I. Zhovtobriukh, N. A. Besley, T. Fransson, A. Nilsson, and L. G. M. Pettersson, *J. Chem. Phys.* **148**, 144507 (2018).
- [25] J. A. Sellberg, T. A. McQueen, H. Laksmono, S. Schreck, M. Beye, D. P. DePonte, B. Kennedy, D. Nordlund, R. G. Sierra, D. Schlesinger, T. Tokushima, I. Zhovtobriukh, S. Eckert, V. H. Segtnan, H. Ogasawara, K. Kubicek, S. Techert, U. Bergmann, G. L. Dakovski, W. F. Schlöter, Y. Harada, M. J. Bogan, P. Wernet, A. Föhlisch, L. G. M. Pettersson, and A. Nilsson, *J. Chem. Phys.* **142**, 044505 (2015).
- [26] P. Wernet, D. Nordlund, U. Bergmann, M. Cavalleri, M. Odellius, H. Ogasawara, L. A. Näslund, T. K. Hirsch, L. Ojamäe, P. Glatzel, L. G. M. Pettersson, and A. Nilsson, *Science* **304**, 995 (2004).
- [27] J. D. Smith, C. D. Cappa, K. R. Wilson, B. M. Messer, R. C. Cohen, and R. J. Saykally, *Science* **306**, 851 (2004).
- [28] A. K. Soper, *Pure Appl. Chem.* **10**, 1855 (2010).
- [29] Y. Kajihara, M. Inui, S. Hosokawa, K. Matsuda, and A. Q. R. Baron, *J. Phys.: Condens. Matter* **20**, 494244 (2008).
- [30] Y. Kajihara, *Rev. High Press. Sci. Tech.* (in Japanese) **26**, 288 (2016).
- [31] G. Ruocco and F. Sette, *Condens. Matter Phys.* **1**, 29 (2008).
- [32] A. Cunsolo, *Adv. Condens. Matter Phys.* **2015**, 137435 (2015).
- [33] F. Sette, G. Ruocco, M. Krisch, C. Masciovecchio, R. Verbeni, and U. Bergmann, *Phys. Rev. Lett.* **77**, 83 (1996).
- [34] S. C. Santucci, D. Fioretto, L. Comez, A. Gessini, and C. Masciovecchio, *Phys. Rev. Lett.* **97**, 225701 (2006).
- [35] A. Angell, *Nature Nanotechnology* **2**, 396 (2007).
- [36] M. H. Cohen and J. Jortner, *Phys. Rev. Lett.* **30**, 699 (1973).
- [37] Y. Tsuchiya and E. F. W. Seymour, *J. Phys.* **C18**, 4721 (1985).
- [38] Y. Tsuchiya, *J. Phys: Condens. Matter* **3**, 3163 (1991).
- [39] D. Ishikawa, M. Inui, K. Matsuda, K. Tamura, S. Tsutsui, and A. Q. R. Baron, *Phys. Rev. Lett.* **93**, 097801 (2004).
- [40] A. Q. R. Baron, Y. Tanaka, S. Goto, K. Takeshita, T. Matsushita, and T. Ishikawa, *J. Phys. Chem. Solids* **61**, 461 (2000).
- [41] T. Yamaguchi, K. Yoshida, N. Yamamoto, S. Hosokawa, M. Inui, A. Q. R. Baron, and S. Tsutsui, *J. Phys. Chem. Solids* **66**, 2246 (2005).
- [42] D. Ishikawa and A. Q. R. Baron, *J. Phys. Soc. Jpn.* **90**, 083602 (2021).
- [43] W. Wagner and A. Pruss, *J. Phys. Chem. Ref. Data* **31**, 387 (2002).
- [44] F. Bencivenga and C. Masciovecchio, *Nuclear Instruments and Methods in Physics Research A* **606**, 785 (2009).
- [45] F. Bencivenga, R. Cucini, F. Capotondi, A. Battistoni, R. Mincigrucci, E. Giangrisostomi, A. Gessini, M. Manfreda, I. P. Nikolov, E. Pedersoli, E. Principi, C. Svetina, P. Parris, F. Casolari, M. B. Danailov, M. Kiskinova, and C. Masciovecchio, *Nature* **520**, 205 (2015).
- [46] A. Q. R. Baron, H. Franz, A. Meyer, R. Ruffer, A. I. Chumakov, E. Burkel, and W. Petry, *Phys. Rev. Lett.* **79**, 2823 (1997).
- [47] M. Saito, M. Seto, S. Kitao, Y. Kobayashi, S. Higashitaniguchi, M. Kurokuzu, M. Sugiyama, and Y. Yoda, *Applied Physics Express* **2**, 026502 (2009).
- [48] M. Saito, S. Kitao, Y. Kobayashi, M. Kurokuzu, Y. Yoda, and M. Seto, *Phys. Rev. Lett.* **109**, 115705 (2012).
- [49] Y. Kajihara, in preparation.

- [50] C. A. Angell, M. Oguni, and W. J. Sichina, *J. Phys. Chem.* **86**, 998 (1982).
- [51] Y. Kajihara, M. Inui, K. Ohara, and K. Matsuda, *J. Phys.: Condens. Matter* **32**, 274001 (2020).
- [52] Y. Katayama, T. Mizutani, W. U. and Osamu Shimomura, M. Yamakata, and K. ichi Funakoshi, *Nature* **403**, 170 (2000).
- [53] V. V. Brazhkin, K. Funakoshi, M. Kanzaki, and Y. Katayama, *Phys. Rev. Lett.* **99**, 245901 (2007).
- [54] J. C. Mauro, P. K. Gupta, and R. J. Loucks, *J. Chem. Phys.* **126**, 184511 (2007).
- [55] Y. Kajihara, N. Shibata, M. Inui, K. Matsuda, and S. Tsutsui, *EPJ Web of Conf.* **151**, 06003 (2017).
- [56] N. Shibata, Y. Kajihara, K. Nukumizu, M. Inui, and S. Tsutsu, in preparation.
- [57] J.-W. Yeh, S.-K. Chen, S.-J. Lin, J.-Y. Gan, T.-S. Chin, T.-T. Shun, C.-H. Tsau, and S.-Y. Chang, *Adv. Eng. Mater.* **6**, 299 (2004).
- [58] Y. F. Ye, Q. Wang, J. Lu, C. T. Liu, and Y. Yang, *Materials Today* **19**, 349 (2016).
- [59] S. C. Santucci, L. Comez, F. Scarponi, G. Monaco, R. Verbeni, J. F. Legrand, C. Masciovecchio, A. Gessini, and D. Fioretto, *J. Chem. Phys.* **131**, 154507 (2009).
- [60] M. D. Ediger, *Annu. Rev. Phys. Chem.* **51**, 99 (2000).